CFD simulations of hydraulic short-circuits in junctions, application to the Grand'Maison power plant

CFD simulations of hydraulic short-circuits in junctions, application to the Grand'Maison power plant

J Decaix[1], J-L Drommi[2], F Avellan[3] and C Münch-Alligné [1,4]

[1] Institute of Sustainable Energy, School of Engineering, HES-SO Valais-Wallis, Rue de l'Industrie 23, 1950 Sion, Switzerland
[2] EDF CIH DT, Chambéry, France
[3] Laboratory for Hydraulic Machines Ecole Polytechnique Fédérale de Lausanne, Avenue de Cour 33 bis, 1007 Lausanne, Switzerland
[4] Institute of Systems Engineering, School of Engineering, HES-SO Valais-Wallis, Rue de l'Industrie 23, 1950 Sion, Switzerland

E-mail: [1]jean.decaix@hevs.ch

Abstract. In the framework of the XFLEX HYDRO H2020 European Project, the pumped-storage power plant of Grand'Maison (France), owned by Electricité De France, focuses on the implementation of the hydraulic short-circuit (HSC) operating mode. This mode increases the flexibility in pumping mode, which helps the integration of intermittent energies. Grand'Maison is divided into two power houses: the first features four Pelton turbine units and the second eight reversible pump-turbines units. A trifurcation splits the flow into three penstocks, each is then split into two branches that feed each power house. The HSC operating mode, which consists in operating the pumps and the Pelton turbines simultaneously, changes the flow paths in the junctions compared to the pump mode. The power plant was not designed to operate in HSC mode over a long duration, therefore an assessment of its feasibility is necessary. 151 computational fluid dynamic simulations are carried out for two bifurcations and one trifurcation. The numerical simulation results show that the local head losses in HSC mode represent less than 1% of the gross head. No flow instabilities are observed at the bifurcations contrary to the trifurcation. Additional analyses are required to better understand the flow in the trifurcation.

1. Introduction

Hydroelectricity is one of the key energy sources for the integration of additional wind and solar energies in the electric power system due to its high flexibility that is still currently improved [1]. Particularly, pumped-storage hydro-power plants (PSP) can deliver in less 100 seconds several GW, making them the only mature solution for large-scale storage capacity [2]. However, the economic environment is reluctant to the development of new PSP mainly in the Alps region [3] despite some new constructions such as Kops II in Austria [4] or Nant de Drance [5] and the extension of existing plants such as Veytaux FMHL+ [6]. The increase in flexibility can be also achieved by extending the operating range of existing power plants or by implementing new operating modes such as the hydraulic short circuit (HSC) mode [7]. The HSC mode consists in operating simultaneously the pump and the turbine by diverting a part of the pumped flow to

the turbine. Consequently, the usually fixed power consumed by the pump is adjusted from the grid point of view. Such a mode is already available in some power plants such as the plants of Kops II [4] and Veytaux FMHL+ [6].

If the HSC mode has been scheduled at the construction of the power plant, the junctions between the different pipes are optimized regarding both the head losses and the development of flow instabilities. For the Kops II project, computational fluid dynamics (CFD) simulations and experiments have been carried out to validate the design of the T-junction [8]. If the HSC mode has not been scheduled as the beginning of the project, the owner of the power plant has to deal with the existing pipes and junctions. CFD and model tests are then used to assess the head losses and the risks of developing flow instabilities.

The T-junction, *i.e.* a junction with an angle of 90° between the pipes, is the most studied junction mainly in the context of nuclear power plants due to thermal fatigue effects [9]. Regarding the hydraulic literature, the main concern is the derivation, based on model scale tests, of analytical formula to calculate the head loss coefficient [10]. For Y-junction, *i.e.* junctions with an angle different from 90° between the pipes, mainly Gardel et al. [11, 12, 13] have proposed formula based on a large number of tests covering angles between 45° and 135°. A more challenging junction is the trifurcation that is often used to divide the flow from the main gallery, connected to the upper reservoir, to three different penstocks that feed into water the hydraulic machines. This junction, if not well designed, can lead to discharge unbalanced between the three penstocks. In [14], the authors considered a trifurcation with a spherical shape and they reported an amplitude of the discharge variation of approximately 30 m^3 s^{-1} in two of the three penstocks, leading to power fluctuations larger than 10 MW. Thanks to CFD simulations, the authors showed that the diameter of spherical trifurcation is responsible of the flow instabilities. They proposed to add guide plates to reduce the diameter of the spherical trifurcation, successfully damping the oscillations. Hyun et al. [15] also investigated a truncated spherical trifurcation (deflection flat plates cut the top and bottom part of the sphere) responsible for a discharge unbalanced between the branches around 14% leading to an output power fluctuation around 18%. CFD simulations show the alternated formation of a vortex at the top and bottom of the trifurcation due to a flow recirculation. By inclining the deflection plates, the flow recirculation is limited and the discharge unbalanced decrease to 11%. On-site, the modification made was more drastic and consisting of adding deflection flat plates to design a pure convergent. Consequently, the output power fluctuations are suppressed. Ruprecht [16] computed also a spherical trifurcation and put in evidence the development of a vortex originated from the top of the trifurcation to one of the lateral branch. Time to time, the vortex "jumps" to the opposite branch. Consequently, the head losses and the discharge values are different from one branch to the other in agreement with the model tests. Aguirre et al. [17] performed CFD simulations of a trifurcation, whose shape is composed of trunk cones. The results show the development of vortices from the top and the bottom walls of the trifurcation. They are responsible for a different repartition of the discharge between the branches ($\approx 40\%$ for the central branch and $\approx 30\%$ for the lateral branches) and discharge fluctuations of 5%. Malik and Paidel [18] performed CFD simulations of a trifurcation to optimize its geometry regarding the head losses. The best geometry is a convergent trifurcation made of trunk cones that does not promote the development of flow instabilities, at least in the simulations.

The CFD investigation of junctions (and mainly trifurcation) in relation with the implementation of a HSC operating mode does not seem to have received a lot of attention, which can be explained by the relative recent use of this operating mode. As part of the European XFLEX HYDRO H2020 project, which aims to demonstrate how more flexible hydropower assets can help countries and regions meet their renewable energy targets, the Grand'Maison pumped storage power plant (France), owned by Electricité De France (EDF), is being considered for the implementation of the HSC operating mode.

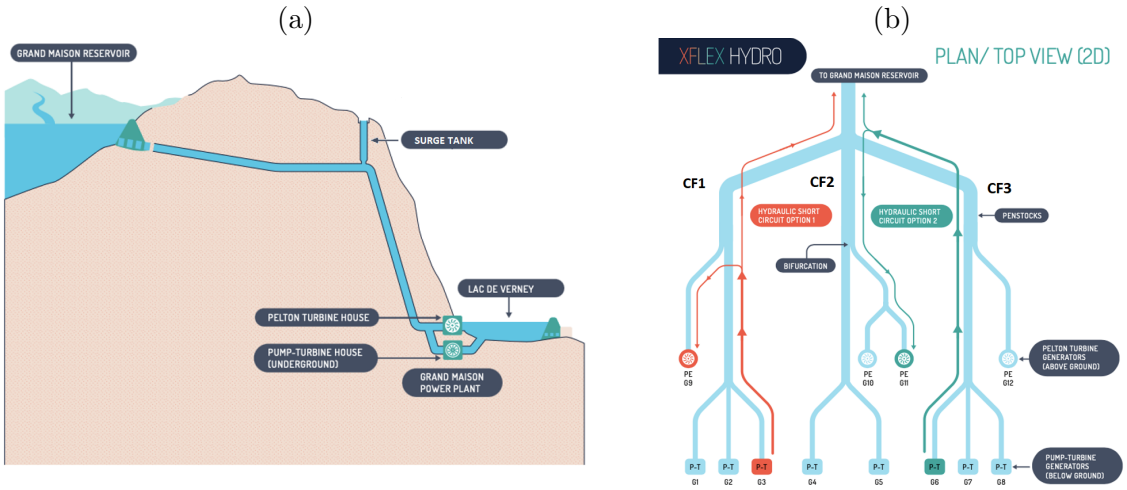

Figure 1. (a): Section view of the Grand'Maison power plant. (b): Schematic representation of the power plant with the three bifurcations and the trifurcation as well as the flow paths for HSC configurations of type 1 (orange) and type 2 (green blue).

The paper focuses on the CFD simulations performed to investigate the influence of the HSC mode on two bifurcations and one trifurcation of the power plant. The main objectives of the simulations are the assessment of the head losses for different HSC configurations and the potential risk of development of flow instabilities in the pipes. The first section describes the Grand'Maison power plant and the flow path considered for the HSC operating mode. Then, the CFD methodology and the results are discussed separately depending if the flow diversion in HSC mode occurs at the bifurcations or at the trifurcation. The paper ends by a conclusion with some perspectives.

2. The Grand'Maison power plant

2.1. Main characteristics

The Grand'Maison power plant is the largest PSP in Europe with 1.8 GW available in turbine mode for a gross head of 922 m and 1.2 GW in pump mode. The power plant is split in two levels (see figure 1a): the first level above the downstream reservoir features 4 Pelton turbines of 156 MW each (currently updated to 170 MW); the second level, underground, features 8 reversible pump-turbines of 156 MW each. A trifurcation distributes the flow from the upper gallery to three penstocks that feeds a different number of Pelton turbines and reversible pump-turbines. The two lateral penstocks, referred as CF1 and CF3 in figure 1b, feed one Pelton turbine and three pump-turbines respectively. The central penstock, CF2, feeds two Pelton turbines and two pump-turbines. The surge tank is located close to the trifurcation as shown in figure 1a. In each penstock, a bifurcation allows distributing the flow either to the Pelton turbine or the pump-turbines. As the number of Pelton turbines and pump-turbines is the same for the lateral penstocks CF1 and CF3, the geometry of the bifurcation is also the same. For the central penstock, the geometry of the bifurcation is different (see figure 2).

2.2. Flow paths in HSC operating mode

Due to the configurations of the pipes, HSC mode can be achieved for various configurations of operation. In figure 1b, two types of HSC configuration are represented:

- Type 1: the HSC takes place between a pump-turbine (in pump mode) and a Pelton turbine located on the same penstock. The red arrows in figure 1b show an HSC configuration

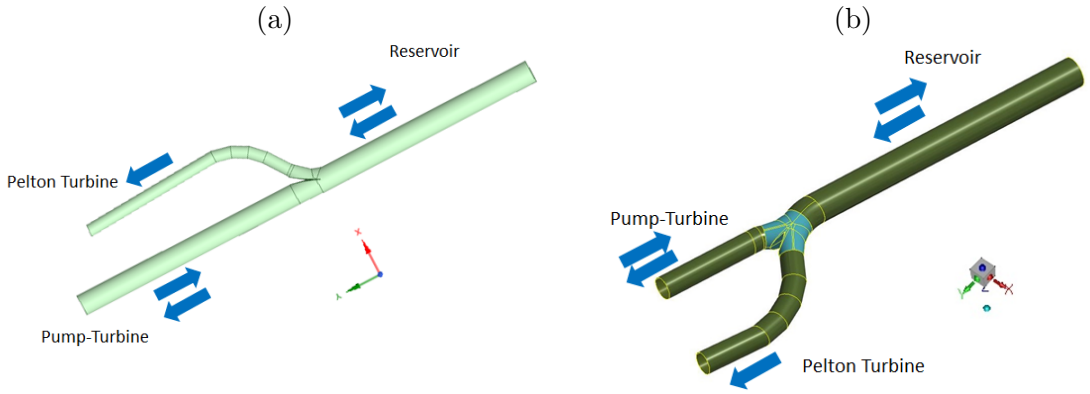

Figure 2. (a): 3D view of the geometry of the bifurcation of the lateral penstocks CF1 or CF3. (b): 3D view of the geometry of the bifurcation of the central penstock CF2. The arrows indicate the possible paths of the flow depending on the operating mode considered.

between the pump-turbine G5 and the Pelton turbine G10 or G11. In this case, the diversion of the flow occurs at the bifurcation.

- Type 2: the HSC takes place between a pump-turbine (in pump mode) and a Pelton turbine located on two different penstocks. The blue arrows in figure 1b show an HSC configuration between the pump-turbine G6 and the Pelton turbine G10 or G11. In this case, the diversion of the flow occurs at the trifurcation.

3. Flow investigation in the bifurcations

3.1. Geometry

The geometry of the two bifurcations, reconstructed from an in-situ 3D-scan, are displayed in figure 2. They look like to a Y-junction, with an alignment between the penstock and the pipe toward the pump-turbines. The main difference between the two bifurcations is the diameter of the branches on the low pressure side of the bifurcation. For the bifurcation of the central penstock, the inner diameter is the same for the pipe toward the pump-turbines and the Pelton turbines with a value of 2.25 m. On the contrary, for the bifurcations on the lateral penstocks the inner diameter of the pipe toward the Pelton turbine is smaller than the one toward the pump-turbines with a value of 1.6 m instead of 2.75 m. The shape of the splitter is also different between the two bifurcations: it is straight for the central penstock and of C-form for the lateral penstocks.

3.2. CFD methodology

The flow numerical simulations of the bifurcations are carried out using the Fluent® software from Ansys®. The fluid is modelled with the Reynolds-Averaged Navier-Stokes (RANS) equations and is solved using a SIMPLEC algorithm. The Reynolds stresses appearing in the RANS equations are closed using the Boussinesq's assumption, which required to determine a scalar eddy viscosity computed using either the realizable $k-\epsilon$ [19] or the RNG $k-\epsilon$ [20] turbulence model. For the HSC operating mode, the boundary conditions have been set in two different ways: either the outlet discharge is set at the outlet of two branches and the total pressure is set at the inlet of the third branch, or the discharge is set at one outlet and at the inlet and the pressure is set at the outlet of the third branch. This CFD set up has been assessed by comparisons with analytical formula derived for T-junctions in a previous publication [21]. In the present paper, it has been applied to compute pump, turbine and HSC operating modes.

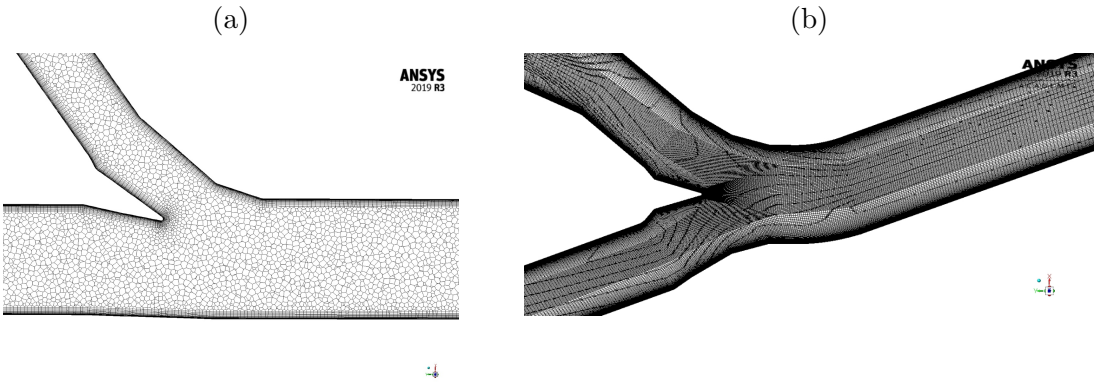

Figure 3. (a): Top view of the poly-core mesh of the bifurcation of the lateral penstocks. (b): Top view of the finest structured mesh of the bifurcation of the central penstock CF2.

Table 1. Characteristic values of the dimensionless wall distance y^+ for each bifurcation.

Bifurcation	Maximum y^+	Maximum of the average y^+	Minimum of the average y^+
CF1 (lateral penstock)	679	147	32
CF2 (central penstock)	525	197	34

Due to the differences in the shape of the two bifurcations, a different meshing strategy is used. A poly-core mesh (see figure 3a) is generated using Fluent Meshing for the bifurcation of the lateral penstocks with 5.2 10^6 nodes and prim layers along the solid walls. Two structured meshes (see figure 3b) are generated using Ansys ICEM CFD$^{\text{TM}}$ for the bifurcation of the central penstock with respectively 4.4 10^6 and 8.2 10^6 nodes. For all the flow configurations considered, the maximum y^+ value is less than 700 and the averaged y^+ value varies between 30 and 200 depending on the operating point simulated (see table 1) for a Reynolds number varying from 1.1 10^6 to 32 10^6.

3.3. Results

In overall, 56 simulations have been carried out for the bifurcation of the penstock CF1 (lateral penstock) and 36 for the bifurcation of the penstock CF2 (central penstock). For each simulations, the local head loss coefficients of the junction between two pipes have been calculated using the equation 1 defined as follows:

$$K_{a-b} = \frac{\Delta p_{tot}}{0.5\,\rho \max\left(C_{rev}\,;\,C_{res}\,;\,|C_{pel}| * H\right)^2} - K_{lin} \tag{1}$$

with:

- K_{a-b} refers to the head loss coefficient between the sections a and b. a and b can take the value rev for the section towards the reversible pump-turbines, res for the section towards the upper reservoir and pel for the section towards the Pelton turbines.
- Δp_{tot} is the difference between the area average total pressure at the inlet of one pipe and the outlet of the second pipe.
- C_{rev}, C_{res} and C_{pel} are the discharge velocity respectively in pipe toward the reversible pump-turbines, the upper reservoir and the Pelton turbine.
- $H = 1$ in HSC mode and 0 otherwise.

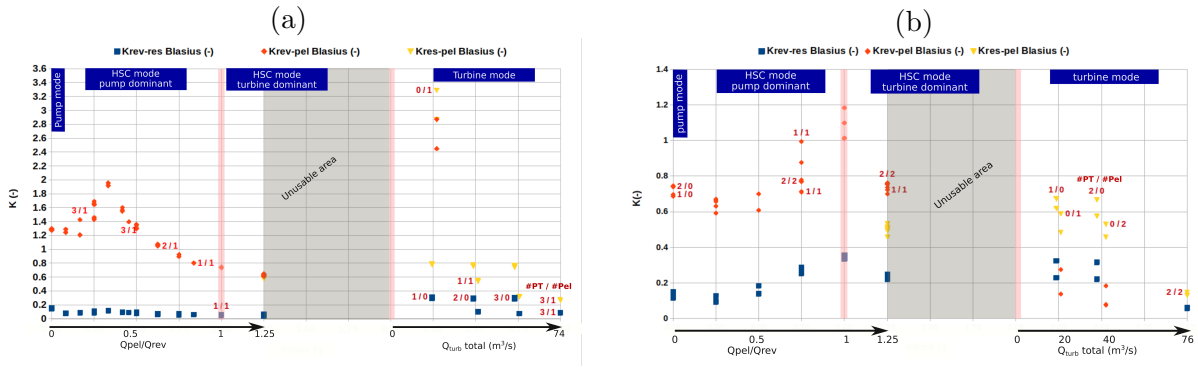

Figure 4. (a): Head loss coefficients for the bifurcation of the penstock CF1 (lateral penstock). (b): Head loss coefficients for the bifurcation of the penstock CF2 (central penstock). The bottom axis is split in two: on the left, the axis refers to the discharge ratio between the Pelton turbine(s) and the pump-turbines; on the right, the axis refers to the discharge turbined. The red numbers give the number of pump-turbines and Pelton turbines in operation.

- K_{lin} is the linear head losses between the inlet or outlet of a pipe and the bifurcation. The linear head losses are computed using the Blasius law, *i.e.* assuming hydraulically smooth flow regime.

The values of the local head loss coefficients K for both bifurcations and for each configuration simulated are shown in 4. The charts have two x-axis. One axis on the left refers to the discharge ratio Q_{pel}/Q_{rev} between the Pelton turbine(s) and the pumps that varies from 0 (equivalent to the pump mode) to 1.25 in HSC mode (the Pelton turbines have a maximum discharge higher than the pumps). A second axis on the right that refers to the discharge in the turbine mode. For each bifurcation, whatever the meshes, the boundary conditions or the turbulence models used, the head loss coefficients collapse on the same curves. The highest discrepancy of 30%, is observed for the bifurcation of penstock CF2 (see figure 4 b) and for a discharge ratio Q_{pel}/Q_{rev} of 0.75. This difference is related to the turbulence model used as shown in [21].

The head loss coefficients have a different behaviour depending on the bifurcation considered. In HSC mode, for the bifurcation of the penstock CF1 (see figure 4a), the head loss coefficient $K_{rev-pel}$, *i.e.* the one between the reversible pump-turbines and the Pelton turbine, is at least 8 times larger than the coefficient $K_{rev-res}$ between the reversible pump-turbines and the upper reservoir. This ratio is only of 3 for the bifurcation of the penstock CF2 (see figure 4b). Moreover, the tendency of the head loss coefficient $K_{rev-pel}$ as a function of the discharge ratio Q_{pel}/Q_{rev} is different. For the bifurcation of the penstock CF1 (see figure 4a), the coefficient $K_{rev-pel}$ increases from 1.2 to 1.9 for a discharge ratio between 0 and 0.3 before decreasing whereas, for the bifurcation of the penstock CF2 (see figure 4b), it decreases from 0.7 to 0.6 for a discharge ratio between 0 and 0.25 before increasing until reaching its maximum value of about 1.1 in pure HSC mode, *i.e.* when the discharge pumped is entirely diverted to the Pelton turbines. In turbine mode, for the bifurcation of the penstock CF1 (see figure 4a), the head loss coefficient $K_{res-pel}$ is at least 3 times larger than the coefficient $K_{rev-res}$. For the bifurcation of the penstock CF2 (see figure 4b), this ratio is around 2. Express in meters, the maximum head losses are reached in HSC mode with a value of 8.5 m for the the bifurcation of the penstock CF1 and 4 m for the bifurcation of the penstock CF2. Compared to the gross head, the head losses represent less than 1%.

The development of flow instabilities downstream the bifurcation in direction to the Pelton turbine(s) is investigated by comparing the helicity contours between the turbine mode and the HSC mode. An example for the bifurcation of the penstock CF2 is shown in figure 5. The

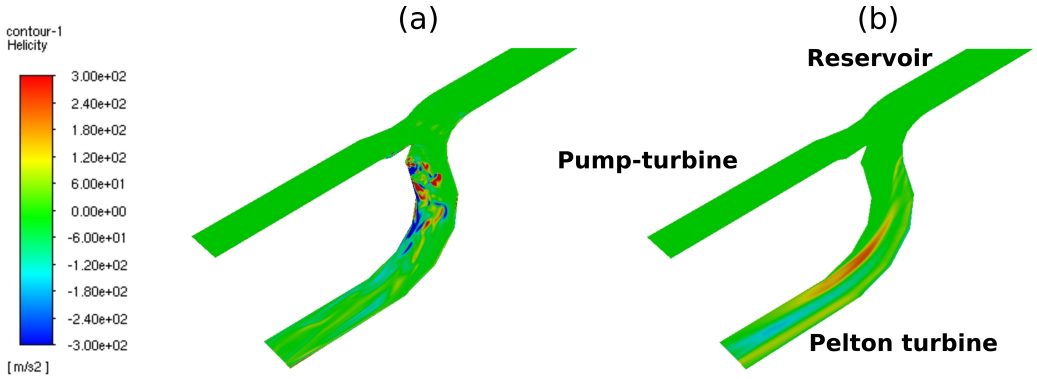

Figure 5. Helicity contours in the mid-plane of the bifurcation of the penstock CF2. (a): HSC operating mode with two pump-turbines and two Pelton in operation and a discharge ratio $Q_{pel}/Q_{rev} = 1.25$. (b): Full discharge turbine mode.

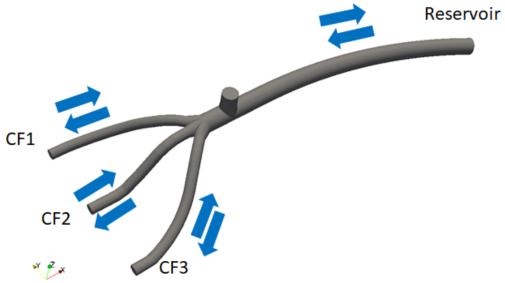

Figure 6. 3D view of the geometry of the trifurcation. The arrows indicate the possible paths of the flow depending on the operating mode considered.

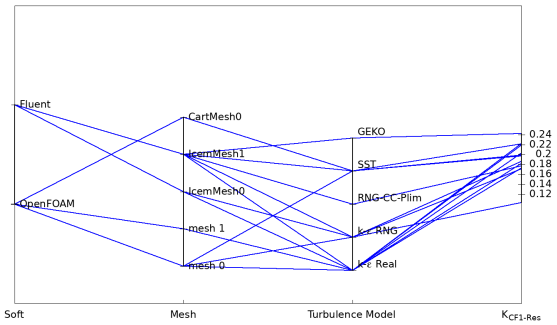

Figure 7. Head loss coefficient $K_{CF1-Res}$ at the trifurcation predicted by each simulation performed in turbine mode.

HSC mode with 2 pump-turbines and 2 Pelton turbines in operation with a discharge ratio Q_{pel}/Q_{rev} of 1.25 is compared with the full discharge turbine mode, *i.e.* 2 Pelton and 2 pump-turbines in operation at their maximum discharge value. In HSC mode, the helicity is large in the elbow of the pipe toward the Pelton turbines. In turbine mode, the helicity is large along elongated regions that corresponds to streamwise vortices extending to the outlet of the pipe. Consequently, the level of helicity in the outlet part of the pipe toward the Pelton turbine is lower in HSC mode than in turbine mode, which suggests a low impact on the Pelton turbines in HSC operating mode. This point has been confirmed by the on-site tests [22].

4. Flow investigation in the trifurcation

4.1. Geometry

The geometry of the trifurcation reconstructed from an in-situ 3D scan is shown in figure 6. The geometry of the surge tank is considered only to the diaphragm in the present investigation. The inner diameter of the upper gallery is equal to 5.4 m whereas the inner diameters of the penstocks are equal to 3 m. The shape of the trifurcation is made of trunk cones as in [17] but compared to this study, the size of the trifurcation is not larger than the diameter of the gallery, which prevents the development of flow instabilities. The splitters between each penstock are of

C-form.

4.2. CFD methodology

The CFD methodology followed for the numerical investigation of the trifurcation is similar to the one used for the bifurcations, with additional simulations performed with the OpenFOAM toolbox v5. By multiplying the simulations using different software, set up, meshes, turbulence models and algorithms for the resolution of the RANS equations, it is possible to have a statistical overview of the CFD results. Figure 7 gives an overview of the CFD methodology followed on the example of the turbine mode. For this operating mode, 13 simulations have been carried out using both Fluent® and OpenFOAM software, 5 meshes (three Cartesian meshes: "mesh 0", "mesh 1" and "CartMesh0" and two tetrahedral meshes: "IcemMesh0" and "IcemMesh1") and 5 turbulence models that are the realizable $k-\epsilon$ model [19], the RNG $k-\epsilon$ model [20], the RNG $k-\epsilon$ model with a production limiter (as applied in [23]) and a curvature correction term [24] (denoted RNG-CC-Plim on the figure), the SST $k-\omega$ [23] and the Generalized $k-\omega$ (GEKO) model [25]. Regarding the meshes, the average y^+ value ranges from 73 for the mesh IcemMesh1 to 768 for the mesh IcemMesh0. Each simulation provides a value for the head loss coefficient between the upstream gallery and the penstock CF1 $K_{CF1-Res}$ (as for the bifurcation, the subscript refers to the sections between which the coefficient is calculated) . Based on these results, average and standard deviation are calculated with a value of 0.2 and 0.02 respectively.

4.3. Results

In overall, 59 simulations have been performed that covers 11 operating points. Whatever the operating point, only the maximum possible discharge value in each penstock is considered. The average and standard deviation of the head loss coefficients for each configuration simulated are summarized in figure 8. Qualitatively, the coefficients have a larger value in HSC modes than in the pump or turbine mode. The highest value reaches 12.5 for the head loss coefficients $K_{CF1-CF2}$ and $K_{CF2-CF3}$ for the HSC configuration 3PTp/2Pel/3PTp, *i.e.* with 3 pump-turbines in pump mode in CF1, 2 Pelton turbines in CF2 and 3 pump-turbines in pump mode in CF3. In HSC mode, the lowest values of the coefficients are obtained for the configuration 1Pel/0/3PTp and its symmetric case 3PTp/0/1Pel. Therefore, the head loss coefficient is lower when the water follows a path with a smaller deviation angle. For instance, the geometric angle is smaller between CF1 and CF3 than between CF1 and CF2. The standard deviation is at least 10 times lower than the average value (for the configuration 1Pel/2Pel/2PTp, the deviation is null because only one simulation has been performed), therefore the maximum deviation is also reached for the case 3PTp/2Pel/3PTp with a value around 1.2. A deviation of 10% between the simulations is not excessive since the head losses are less than 0.5% of the gross head.

Figure 9 compares the contours of the velocity magnitude in the mid-plane of the trifurcation between the RNG and realizable $k-\epsilon$ turbulence models for the configuration 3PTp/2Pel/3PTp. The realizable model predicts a steady flow with a detachment of the flow in the gallery. On the contrary, the RNG model provides rather the topology of an "unsteady" flow.

Preliminary unsteady simulations seem to confirm this difference as shown in figure 10, where the time history of the total pressure at each inlet and outlet of the computational domain for simulations with either the RNG $k-\epsilon$ or the realizable $k-\epsilon$ turbulence model is shown. Mainly in the penstocks CF1 and CF3, the total pressure predicted by the realizable $k-\epsilon$ model oscillates weakly contrary to the one predicted by the RNG $k-\epsilon$ model. The fast Fourier transform of the signals from the penstock CF1 evidences a low frequency at approximately 0.2 Hz in both cases but with an amplitude of 2500 Pa, equivalent to a peak to peak variation of 0.5 m, for the RNG $k-\epsilon$ model and 200 Pa for the realizable $k-\epsilon$. The presence of such a low frequency could interfere with the control of the machines if it leads to a change in the operating point. However, additional investigations are required to assure the existence of such oscillations.

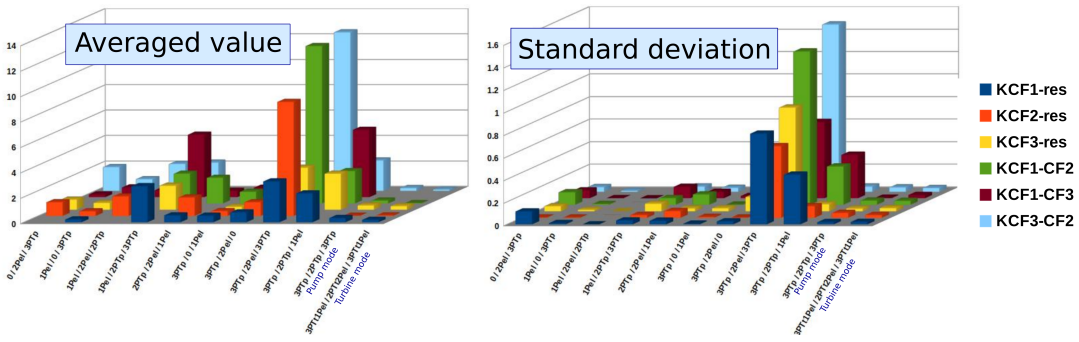

Figure 8. Average and standard deviation of the head loss coefficients for each configuration simulated. The operating point are defined by the number of machines in operation in each penstock, for instance the case 3PTp/2Pel/3PTp refers to the HSC mode with 3 pump-turbines in pump mode in CF1, 2 Pelton turbines in CF2 and 3 pump-turbines in pump mode in CF3. The acronyms are as follows: PTp stands for pump-turbine in pump mode, PTt for pump-turbine in turbine mode, Pel for Pelton turbine. The turbine and pump modes are specified, the other operating points are HSC modes.

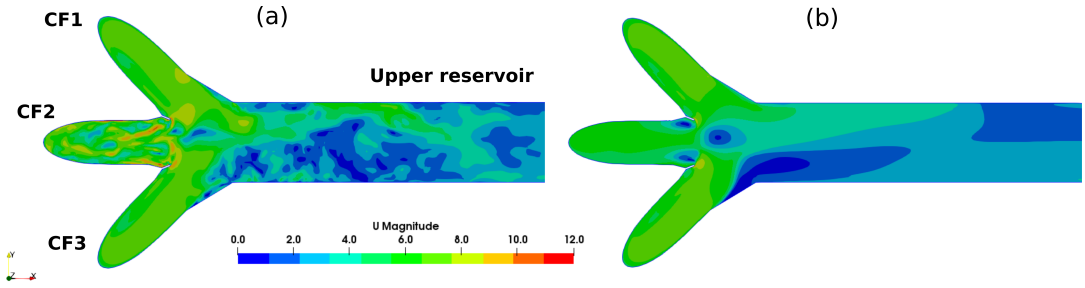

Figure 9. Top view of the contours of the velocity magnitude (in m/s) in the mid-plane of the trifurcation for the configuration 3PTp/2Pel/3PTp. OpenFOAM steady simulations on the mesh "mesh 0" wit a discharge imposed at the CF1, CF2, CF3 and a pressure at the upper reservoir. (a): RNG $k-\epsilon$. (b): realizable $k-\epsilon$.

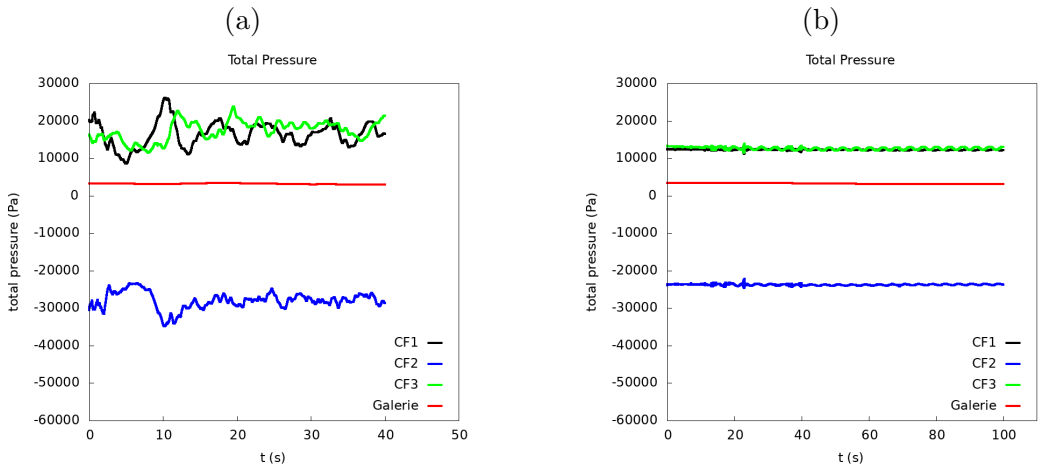

Figure 10. Time evolution of the total pressure at each inlet and outlet of the trifurcation. (a): RNG $k-\epsilon$ turbulence model. (b): realizable $k-\epsilon$ turbulence model. OpenFOAM unsteady simulations on the mesh "mesh 0".

5. Conclusion

CFD simulations of the flow in different junctions of the Grand'Maison power plant have been carried out to investigate the head losses and the flow instabilities in HSC mode. Due to the lack of measurements, the methodology followed consists in performing simulations with different meshes, boundary conditions and turbulence models. Then, comparisons and statistical analyses of the CFD results allows the extraction of the head loss coefficients with a certain interval of confidence. For all the junctions, even if the head losses increase in HSC mode compared to the turbine and pump modes, the head losses never exceed 1% of the gross head, which is lower than the head losses in the penstocks. Another topic of interest is the development of flow instabilities. For the bifurcations, no large instabilities are observed in HSC mode compared to the standard pump and turbine modes. For the trifurcation, the conclusion is more fuzzy since for at least one HSC configuration, low frequency oscillations of the total pressure are observed mainly in the lateral penstocks. However, the amplitude of the oscillations is strongly dependent on the turbulence model used. Therefore, additional analyses are required to determine if the oscillations are likely to actually occur and could have an influence on the operation of the machines. Specific on-site test can been planned to check this potential risk.

Acknowledgments

The Hydropower Extending Power System Flexibility (XFLEX HYDRO) project has received funding from the European Union's Horizon 2020 research and innovation programme under grant agreement No 857832.

References

[1] Kougias I, Aggidis G, Avellan F, Deniz S, Lundin U, Moro A, Muntean S, Novara D, Pérez-Díaz J I, Quaranta E, Schild P and Theodossiou N 2019 *Renewable and Sustainable Energy Reviews* **113** 109257
[2] Guittet M, Capezzali M, Gaudard L, Romerio F, Vuille F and Avellan F 2016 *Energy* **111** 560–579
[3] Gurung A B, Borsdorf A, Füreder L, Kienast F, Matt P, Scheidegger C, Schmocker L, Zappa M and Volkart K 2016 *Mountain Research and Development* **36** 222–232
[4] Meusburger P 2009 Kops II on the grid – first experiences and lessons learned
[5] Seingre G, Ihly T and Frei H R 2011 *Geomechanics and Tunnelling* **4** 627–642
[6] Micoulet G, Jaccard A and Rouge N 2016 *Hydro2016*
[7] Pérez-Díaz J I, Chazarra M, García-González J, Cavazzini G and Stoppato A 2015 *Renewable and Sustainable Energy Reviews* **44** 767–784
[8] Huber B, Korger H and Fuchs K 2005 *XXXI IAHR Congress*
[9] Smith B, Mahaffy J and Angele K 2013 *Nuclear Engineering and Design* **264** 80–88
[10] Rennels H 2012 *Pipe Flow* (John Wiley & Sons) ISBN 0470901020
[11] Gardel A 1957 *Bulletin technique de la Suisse romande* 123–130
[12] Gardel A 1957 *Bulletin technique de la Suisse romande* 143–148
[13] Gardel A and Rechsteiner G F 1970 *Bulletin technique de la Suisse romande* 363–391
[14] Guo X, Cheng H, Wang H, Cheng Y and Sun M 2019 *Energies* **12** 2941
[15] Hyun J J, Choi J W, Jang W G, Cho Y, Kim Y I, Cho T Y, Cho I J and Kim Y J 2019 *IOP Conference Series: Earth and Environmental Science* **240** 052017
[16] Ruprecht A 2006 *High Performance Computing on Vector Systems* (Springer Berlin Heidelberg) pp 155–169
[17] Aguirre C A, Camacho R G R, de Oliveira W and Avellan F 2019 *Renewable Energy* **131** 197–207
[18] Malik R K and Paudel P 2009 *Hydro Nepal: Journal of Water, Energy and Environment* **5** 56–61
[19] Shih T H, Liou W W, Shabbir A, Yang Z and Zhu J 1995 *Computers & Fluids* **24** 227–238
[20] Yakhot V, Orszag S A, Thangam S, Gatski T B and Speziale C G 1992 *Physics of Fluids A: Fluid Dynamics* **4** 1510–1520
[21] Decaix J, Biner D, Drommi J L, Avellan F and Münch-Alligné C 2021 *IOP Conference Series: Earth and Environmental Science* **774** 012013
[22] Drommi J L 2021 *WORLD HYDROPOWER CONGRESS 2021*
[23] Menter F R 2009 *International Journal of Computational Fluid Dynamics* **23** 305–316 ISSN 1061-8562
[24] Smirnov P E and Menter F R 2009 *Journal of Turbomachinery* **131** 041010 ISSN 0889504X
[25] Menter FR and Lechner R and Matyushenko A 2019 Best Practice : Generalized k-ω Two-Equation Turbulence Model in ANSYS CFD (GEKO) Tech. rep. ANSYS